TRR
JOURNAL OF THE TRANSPORTATION RESEARCH BOARD

Research Article

Transportation Research Record
1–15

DOI: 10.1177/03611981231192999
journals.sagepub.com/home/trr
Sage

Characterizing Human–Automated Vehicle Interactions: An Investigation into Car-Following Behavior

Yanlin Zhang[1] **and Alireza Talebpour**[1]

Abstract

Automated vehicles are expected to influence human drivers' behavior. Accordingly, capturing such changes is critical for planning and operation purposes. With regard to car-following behavior, a key question is whether existing car-following models can replicate these changes in human behavior. Using a data set that was collected from the car-following behavior of human drivers when following automated vehicles, this paper offers a robust methodology based on the concept of dynamic time warping to investigate the critical parameters that can be used to capture changes in human behavior. The results indicate that spacing can best substantiate such changes. Moreover, calibration and validation of the intelligent driver model (IDM) suggest its inability to capture changes in human behavior in response to automated vehicles. Thus, an extension of the IDM that explicitly models stochasticity in the behavior of individual drivers is applied, and the results show such a model can identify a reduction in uncertainty when following an automated vehicle. This finding also has implications for a stochastic extension to other models when analyzing and simulating a mixed-autonomy traffic flow environment.

Keywords

operations, automated/autonomous vehicles, traffic flow

Automated vehicles (AVs) have increased their presence in the emerging mobility system through their ability to sense, evaluate, and predict the surrounding environment meticulously, navigate and plan trajectories comprehensively, and accurately perform the corresponding maneuvers. Based on their improved performance with regard to perception, motion planning, and control compared with human drivers, AVs have the potential to revolutionize future mobility in a fundamental way by promoting safety (*1*–*3*), increasing throughput and maintaining stability (*4*), reducing emissions (*5*, *6*) and fuel consumption (*7*), and providing critical mobility to the elderly and disabled (*8*). The AV industry has also burgeoned since technology giants, such as Google's Waymo and transportation network company leaders Uber and DiDi, began collaborating and competing with the traditional automobile manufacturers, for example, General Motors and Ford (*9*).

Despite all the potential advantages AVs offer, full market penetration is beyond their scope in the near future (*10*); accordingly, a mixed traffic environment with different levels of autonomy is expected in a transition phase. The behavior of humans and AVs are known to be fundamentally different because each follows different logic and mechanisms. Therefore, utilizing the benefits of AVs hinges on characterizing the interactions between humans and AVs in mixed-autonomy traffic.

When investigating AVs' influence on traffic flow, early research focused on the unique features of AVs and the corresponding implications for macroscopic characteristics of traffic flow. Rajamani and Shladover (*11*) conducted a comparative experimental study on the minimum time headway between human-driven vehicles and AVs. The results suggested that AVs can maintain a shorter time gap, which implies a potential increase in capacity. Chen et al. (*12*) provided a theoretical

[1]Department of Civil and Environmental Engineering, University of Illinois at Urbana-Champaign, Urbana, IL

Corresponding Author:
Alireza Talebpour, ataleb@illinois.edu

formulation of equilibrium operational capacity in mixed-autonomy traffic, considering AVs' penetration rate, platoon size, spacing characteristics, and lane policies. In another study, Talebpour and Mahmassani (*4*) presented a comprehensive acceleration model and a simulation framework to shed light on traffic flow dynamics, including stability and throughput under different market penetration rates, when both connected and AVs were involved.

In analyzing the interactions between humans and AVs, many previous studies have focused on AV operations but rather overlooked the possible behavioral changes in human drivers. For example, Van Arem et al. (*13*) extended adaptive cruise control to cooperative adaptive cruise control (CACC) by allowing information exchange via wireless communication, and proposed a safe acceleration logic. Later, Wang et al. (*14*) presented a car-following model for CACC that considered more vehicles in the platoon. However, the above studies did not model human drivers' behavior explicitly. Therefore, until recently, the question of whether and to what extent the introduction of AVs will influence the behavior of human drivers remained uncertain. Among all the decisions that define vehicle interactions, car-following, which dictates how vehicles accelerate in response to the speed, distance, or relative velocity of surrounding vehicles, is probably the most basic. Thus, the studies that focused on human–AV interactions mainly considered the car-following behavior itself, and did not take more complex behavior such as lane changing into account. Cui et al. (*15*) investigated the possibility of a single AV stabilizing the traffic flow, assuming human drivers maintained their behavior patterns. Later, Stern et al. (*16*) designed an experiment on a circular track with a single AV in the platoon and provided evidence of AVs' ability to dampen stop-and-go waves, even with a less than 5% market penetration rate. This series of works demonstrated that AVs could increase traffic flow stability by preventing shock wave formation and spread. In a more recent study, Zhao et al. (*17*) performed car-following experiments to compare human-following-human and human-following-AVs, and the results indicated that subjective trust in AV technologies would have an impact on driver behavior. Under different experimental settings, Rahmati et al. (*18*) conducted an empirical study with a three-vehicle fleet focusing on the human drivers in human–AV interactions. A series of comparative car-following experiments revealed the existence of behavioral changes in human drivers after the introduction of AVs. Zheng et al. (*19*) then showed in simulation that the uncertainty in human drivers' behavior decreases as the penetration rate of AVs increases.

One of the key aspects missing from studies focusing on human–AV interactions is the ability of car-following models to capture such changes in behavior and the accurate modeling of human behavior in response to AVs. Indeed, the previous studies remain silent on the evaluation and validation of the ability of car-following models to capture such behavioral changes effectively. Therefore, an investigation of the existing models, especially those commonly used by researchers and practitioners, will complement the literature and will be essential in characterizing human–AV interactions. To address the aforementioned questions, the major contribution of this study is to investigate whether commonly used models in non-AV traffic can capture human drivers' behavioral changes, and if not, what special considerations and extensions to the models are needed. These findings can provide insights for characterizing human–AV interaction and will increase the reliability of simulation frameworks in modeling mixed traffic.

The paper is organized as follows. The next section elaborates on the experiment and data utilized in this study. Following this, the methodologies employed are described: a data-driven dynamic time warping (DTW) analysis to examine the behavioral difference between following an AV and a human-driven vehicle that includes speed, acceleration, relative speed, spacing, and time headway; and a model-based method to calibrate and validate stochastic car-following models. The data-driven DTW analysis will investigate which drivers' behavior measurements can best substantiate changes in driver behavior, and the model-based method will further examine whether car-following models can capture such changes. The paper then presents the results and an associated discussion. Finally, the paper concludes with some summary remarks and offers a few suggestions for future research.

Data Description

This section is a brief version of the experimental setup described in Rahmati et al. (*18*). To model the potential impact of AVs on human drivers in mixed traffic, previous studies have focused mainly on capacity analysis. For example, Chen et al. (*12*) classified car-following into four scenarios to formulate the equilibrium capacity based on whether the leader and follower vehicle were automated. This modeling technique also provides insights for designing a car-following experiment to compare the different behavior patterns when a human is following an AV or another human-driven car (H).

This study utilizes the data collected by Rahmati et al. (*18*). Figure 1 shows the vehicle platooning settings in their experiment. Two scenarios were defined to study the human drivers' behavior when the leading vehicle was automated or conventional. In both scenarios, the control vehicle (vehicle 1) was driven by the same driver

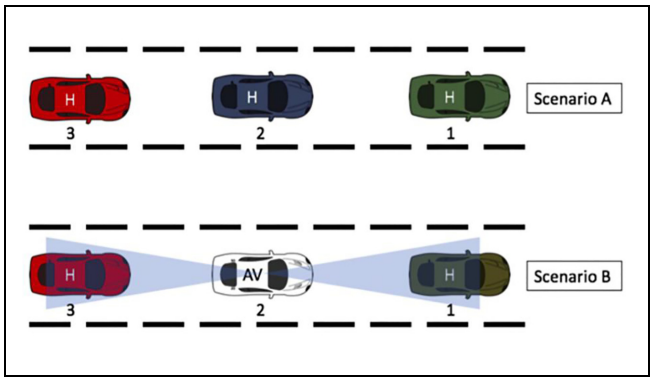

Figure 1. Data collection scenarios (*18*).
Note: H = human-driven car; AV = automated vehicle.

who followed a fixed speed profile to preserve the consistency in other latent variables in each experiment. The follower (vehicle 3) was the test object in each experiment, and the measurements of the driver's behavior were documented as time series data. The leader (vehicle 2) was operated differently between the two scenarios. In scenario A, the leader (vehicle 2) executed the speed profile of a human driver, whereas in scenario B, the vehicle executed the speed profile of an AV. To generate realistic speed profiles for vehicles 1 and 2, five leader–follower pair trajectories were extracted from the NGSIM US-101 data set (*20*). Moreover, the speed profile for the AV in scenario B was determined by a deterministic acceleration modeling framework determined by Van Arem et al. (*13*) and represented by the following equation:

$$a_n^d(t) = k_a a_{n-1}(t-\tau) + k_v(v_{n-1}(t-\tau) - v_n(t-\tau)) + k_d(s_n(t-\tau) - s_{ref}) \quad (1)$$

where $a_n^d(t)$ is the acceleration of vehicle n in meters per square second, v_n is the speed of vehicle n in meters per second, τ is the reaction time in seconds, s_n is the spacing in meters, s_{ref} is the maximum among the safe following distance s_{safe}, the following distance based on the reaction time s_{system}, and the minimum distance s_{min}, which is set to 2.0 m in Van Arem et al. (*13*). s_{safe} and s_{system} are computed as follows:

$$s_{safe} = \frac{v_{n-1}^2}{2}\left(\frac{1}{a_n^{dec}} - \frac{1}{a_{n-1}^{dec}}\right) \quad (2)$$

$$s_{system} = v_n\tau \quad (3)$$

where n and $n-1$ represent the AV and its leader, respectively, a_n^{dec} is the deceleration of vehicle n in meters per square second, and $k_a = 1.0$, $k_v = 0.58$, and $k_d = 0.1$ are model parameters whose values were recommended in Van Arem et al. (*13*).

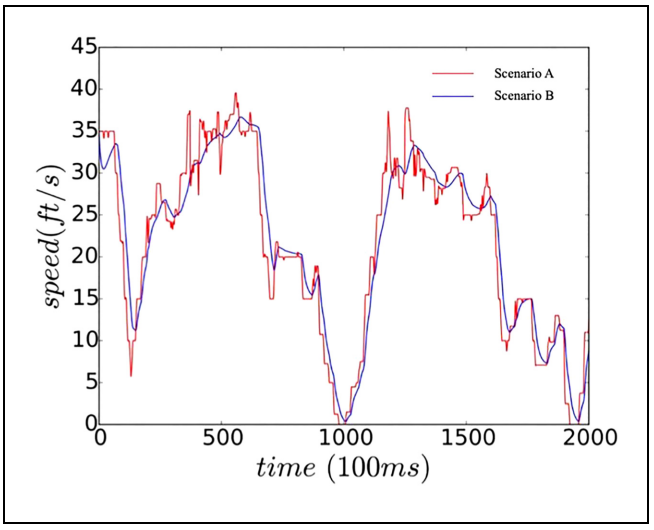

Figure 2. Sample speed profile for vehicle 2 under the two scenarios (*18*).

To account for the range limitation of the sensors and the maximum deceleration for the AV and its leader, the maximum safe speed v_{max} is defined by the following equations:

$$\Delta x_n = (x_{n-1} - x_n - l_{n-1}) + v_n\tau + \frac{v_{n-1}^2}{2a_{n-1}^{dec}} \quad (4)$$

$$\Delta x = \min\{r, \Delta x_n\} \quad (5)$$

$$v_{max} = \sqrt{-2a_i^{dec}\Delta x} \quad (6)$$

where x_n is the location of vehicle n, l_n is the length of vehicle n, r is the sensor detection range (note that r is set to 90 m in Rahmati et al. [*18*]), and a_i^{dec} is the maximum deceleration of vehicle n. Finally, the acceleration of the AV at time t is computed as follows:

$$a_n(t) = \min\{a_n^d(t), k(v_{max} - v_n(t))\} \quad (7)$$

where k is a model parameter, and $k = 1.0$ as given in Rahmati et al. (*18*).

The speed profile in scenario A is drawn directly from lead–follower pairs in the NGSIM US-101 data set to represent human drivers, and in scenario B, the NGSIM data are taken as inputs to compute the corresponding speed profile based on Equations 1 through 7. The speed profile of an AV shares a similar pattern to a human-driven vehicle but it is generally smoother, as shown in Figure 2.

The experiment was performed on the AV testing track at Texas A&M University's RELLIS campus, with nine drivers operating the test object vehicle (vehicle 3 in

Figure 1) under the two scenarios and five different speed profiles. The AV used in this study was Texas A&M University's automated Chevy Bolt, which can follow any given speed profile. Other vehicles used were conventional cars with no automation. To avoid any bias during experiments, the drivers of the test object vehicle were not aware of the type of their leading car during experiments, and they were simply told to follow the leader along a given straight route. The driving behavior measurements, including speed, acceleration, location, spacing, time headway, and relative speed (the velocity difference between vehicle 2 and 3), were collected at a frequency of 10Hz. After preprocessing, 45 samples in scenario A and 44 samples in scenario B remained. For more information about the data collection, please refer to Rahmati et al. (*18*).

Methodology

This section presents two steps for addressing whether an extension to non-AV models is needed to capture the behavioral change of human drivers in mixed traffic. The first step is a data-driven analysis to measure the difference between the two scenarios (i.e., human-following and AV-following), and the second step is a model-based method to investigate how capturing stochasticity in human decision-making has an impact on the ability of the models to capture such behavioral changes.

Data-Driven Method: DTW Analysis

The drivers' behavior consists of a collection of time series data, including (a) speed, (b) acceleration, (c) longitudinal locations, (d) relative speed, (e) spacing, and (f) time headway. An intuitive way of measuring the difference between following a human-driven vehicle and an AV is to use the Euclidean distance, and according to Esling and Agon (*21*), the Euclidean distance and other L_p norms have been the most popular metrics. For example, taking the longitudinal locations, given two sets of experimental results under two car-following scenarios with driver i and speed profile j, this paper follows the definition of the Euclidean distance of locations presented by Rakthanmanon et al. (*22*).

$$ED_{ij}^{x}\left(X_{ij}^{H}, X_{ij}^{AV}\right) = \sqrt{\sum_{t}\left(x_{ij}^{H}(t) - x_{ij}^{AV}(t)\right)^2} \qquad (8)$$

where i is the index of drivers ($i = 1, 2, ..., 9$), j is the index of speed profiles ($j = 1, 2, ..., 5$), $x_{ij}^{H}(t)$ is the longitudinal locations following a human-driven vehicle at time t, and $x_{ij}^{AV}(t)$ is the longitudinal locations following an AV at time t. Here, the two location trajectories being compared are truncated into the same length before evaluating the distance, which means only those data points with the same time t will be considered in Equation 8.

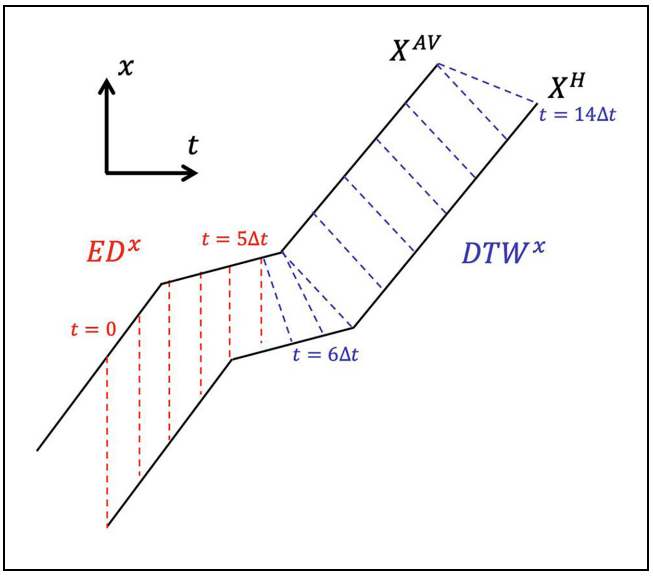

Figure 3. Illustration of the computational difference between the Euclidean distance (red dotted lines from $t = 0$ to $t = 5\Delta t$) and dynamic time warping (blue dotted lines from $t = 6\Delta t$ to $t = 14\Delta t$).

However, the Euclidean distance may not suffice to quantify the difference between the collected time series data in this study for two reasons. The first is the inability to measure the dissimilarity of time series with different lengths accurately, which is an innate shortcoming of Euclidean distance (*22*). If the Euclidean distance were to be used as the metric in the illustrative example in Figure 3, all the information contained in the data points in X^{AV} before $t = 0$ would be lost. There is no guarantee that each driver spends the same amount of time during experiments when following an AV or a human-driven car. Indeed, the drivers were told to follow the leader without more information or instructions to ensure unbiasedness. Therefore, the two time series being compared may not have identical lengths, which leads to early termination according to Equation 8; thus, the result is made smaller by not accounting for all data points. Second, from the collected data, time series data may share similar patterns and extreme values, but one is shifted along the time axis; in this case, Equation 8 will yield an unrealistically large value. More elaborations on the above issues will be given in the following analysis and in the numerical results in the Results and Analysis section.

Figure 3 demonstrates why the Euclidean distance has intrinsic shortcomings in evaluating the differences in time series data accurately. Here, X^{AV} and X^{H} are similar to each other but out of phase (i.e., with a time delay).

When Equation 8 is used to compute the difference, data points at the start of x^{AV} are not included, and the matching patterns between two turning points (from $t = 3\Delta t$ to $t = 9\Delta t$) are not finely captured. To address this shortcoming, another alignment technique different from one-to-one vertical matching called DTW is utilized to evaluate the difference in human drivers' behavior when following an AV as opposed to another human-driven vehicle. Bellman and Kalaba (*23*) first raised the idea of matching the time series among sections by locally warping the time axis, and it is now commonly used in time series data mining (*24*).

In the light of DTW's ability to calculate the optimal matching and measure the difference in time series data, following the guidelines provided by Hosseini et al. (*25*), this study develops a DTW formulation to quantify the behavioral changes in human drivers when following an AV. For a given driver and speed profile, denote A and H as driving behavior (e.g., speed) time series data following an AV or human-driven vehicle, respectively ($A = [a_1, a_2, a_3, \ldots, a_m]$ and $H = [h_1, h_2, h_3, \ldots, h_n]$). Here, m and n are the magnitudes. Because $m, n \in \mathbb{N}$ and are not necessarily equal, the **local cost matrix** $D \in \mathbb{R}^{m \times n}$ is defined to find the optimal matching:

$$D \in \mathbb{R}^{m \times n} : d_{ij} = \| a_i - b_j \| = \sqrt{(a_i - b_j)^2}, \quad i \in [1:m], j \in [1:n] \tag{9}$$

where d_{ij} is an element in the local cost matrix D.

Based on the local cost matrix, a **warping path** ($W = [w_1, w_2, w_3, ..., w_k, ..., w_K]$), represents a set of mapping relationships between A and H. An element in the warping path $w_k = (i_k, j_k) \in [1:m] \times [1:n]$ means a_{i_k} and h_{j_k} form a pair in the optimal matching. Therefore, the objective function in this DTW formulation is as follows:

$$DTW(A,H) = \min_W \sqrt{\sum_{k=1}^{K} d^2_{i_k j_k}}. \tag{10}$$

where $DTW(A,H)$ is the **DTW distance**, defined in Senin (*24*) and $d_{i_k j_k}$ is the (i_k, j_k) -th elements in the local cost matrix D.

The DTW distance is the accumulated total cost of the optimal warping path. In contrast to the Euclidean distance calculated by Equation 8, the DTW distance is computed based on optimal matching, which will yield more plausible measurements in the difference between time series A and H. The constraints are as described in Senin (*24*):

$$w_1 = (1,1), \tag{11}$$

$$w_K = (m,n), \tag{12}$$

$$(i' - i) \leqslant 1, \forall w_k = (i,j), w_{k+1} = (i',j'), \tag{13}$$

$$(j' - j) \leqslant 1, \forall w_k = (i,j), w_{k+1} = (i',j'), \tag{14}$$

$$(i' - i) \geqslant 0, \forall w_k = (i,j), w_{k+1} = (i',j'), \tag{15}$$

$$(j' - j) \geqslant 0, \forall w_k = (i,j), w_{k+1} = (i',j'), \tag{16}$$

The given six constraints instantiate three key assumptions first formally proposed by Sakoe and Chiba (*26*): (a) **Boundary assumption**: Equations 11 and 12 ensure the warping path starts at the first point and ends at the last point of the two time series, which is an assumption of alignment in DTW; (b) **Continuous assumption**: Equations 13 and 14 ensure a match with neighboring points, which implies that every time step should be included in the optimal warping path; and (c) **Monotonous assumption**: Equations 15 and 16 preserve the time orders and essentially make sure time does not go backward.

So, the optimization problem defined by Equations 10 through 16 is reduced to a shortest path problem given the sink, source, and edge costs. The Bellman–Ford algorithm is suitable for solving such problems, and to address the constraints, a dynamic programming (DP) method is used. Denote the **cumulative distance** as $c(i,j)$, which represents the sum of local cost along the warping path from (1, 1) to (i,j). Then, the recurrent relationship for this DP is as follows:

$$c(i,j) = d_{ij} + \min\{c(i-1,j-1), c(i-1,j), c(i,j-1)\} \tag{17}$$

The pseudo-code for the DP algorithm in computing the cumulative distance matrix $C \in \mathbb{R}^{m \times n}$ described in Senin (*24*) is presented below.

Algorithm 1 CumulativeDistanceMatrix(A,H,D)

```
m ← ‖ A ‖
n ← ‖ H ‖
New array C[1...m, 1...n]
Initialize C[1, 1] = 0
for i = 1; i⩽m; i ++ do
    C[i, 1] ← C[i − 1, 1] + D[i, 1]
end for
for j = 1; j⩽n; j ++ do
    C[1, j] ← C[1, j − 1] + D[1, j]
end for
for i = 1; i⩽m; i ++ do
    for j = 1; j⩽n; j ++ do
        C[i, j] ← D[i, j] + min{C[i − 1, j − 1],
                               C[j − 1, j], C[i, j − 1]}
    end for
end for
Return C
```

Table 1. A Piece-Wise Linear Speed Example for the $ED(V^{AV}, V^{H})$ and $DTW(V^{AV}, V^{H})$ Calculations

Time (s)	20	22	24	26	28	30	32	34	36	38	40	42	44
Speed following a human-driven vehicle (km/h)	14	18	22	26	20	14	8	2	8	14	20	26	NA
Speed following an AV (km/h)	NA	8	13	18	23	19	15	11	7	3	9	15	21

Note: AV = automated vehicle; NA = not available.

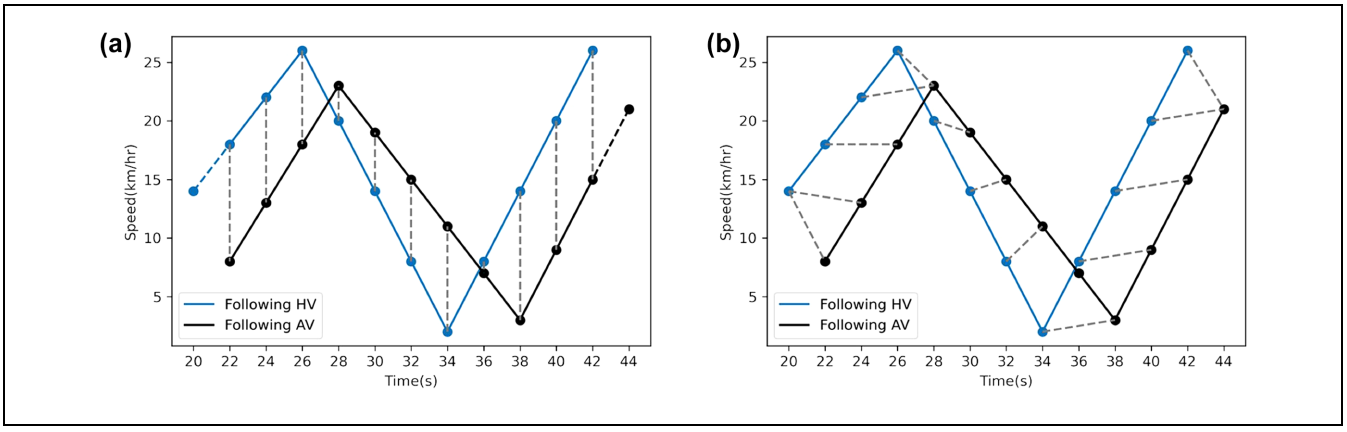

Figure 4. Matching patterns for the Euclidean distance and the DTW distance of speed, respectively: (*a*) $ED(V^{H}, V^{AV})$; and (*b*) $DTW(V^{H}, V^{AV})$.
Note: DTW = dynamic time warping; H = human-driven car; AV = automated vehicle.

To compute the local cost matrix $D \in \mathbb{R}^{m \times n}$ as an input to the above algorithm, a time complexity of $O(mn)$ is expected. It is clear that algorithm 1 also runs in $O(mn)$, and can calculate the cumulative distance matrix $C \in \mathbb{R}^{m \times n}$ correctly. Given the cumulative distance matrix, the optimal warping path W can be recovered in $O(n)$ time by tracing back from $C[m, n]$. Thus, the total runtime is in $O(mn)$.

Table 1 shows an example of two time series containing speed information. This pair of speed data is a piecewise linear approximation from the experiment data by driver No. 1 under speed profile 334. Each speed series spans over 22 s and has 12 time steps. Following the definition of the Euclidean distance and the approach to calculating it provided in the seminal work by Rakthanmanon et al. (*22*), only paired data occurring at the same time in both time series will be used for computing distances. Figure 4 shows the matching patterns in the Euclidean distance. Eleven pairs of points are plugged into Equation 8, which yields $ED\left(V^{AV}, V^{H}\right) = 27.80 km/hr$. For the DTW distance, the optimal matching pattern is calculated by solving the shortest path problem in the local distance matrix. Fourteen pairs of points are included in the calculation, as shown in Figure 4. According to the definition of DTW distance in Equation 10, the result is $DTW\left(V^{AV}, V^{H}\right) = 9.38 km/hr$. The DTW distance evaluation includes all the data points, and the first and last time steps are truncated for the Euclidean distance.

From this simplified example, the evaluation process indicates that the DTW distance has an advantage over the Euclidean distance in measuring the difference between two time series with different lengths but similar patterns, which is a feature of the empirical data set utilized in this paper. Because Rahmati et al. (*18*) have revealed the existence of changes in human behavior in mixed traffic, this study aims to identify which behavioral parameter(s) (i.e., acceleration, speed, relative speed, spacing, and time headway) can best substantiate such changes using the DTW analysis framework. However, two normalization steps are still needed to compare different behavior parameters with heterogeneous lengths and units.

The DTW distance is an accumulation of errors, so longer time series data inherently have a larger DTW distance, and using the DTW distance defined in Equation 10to measure the difference between two scenarios directly may yield biased results. To address this issue, Giorgino (*27*) defined the **length-normalized DTW distance (NDTW)** as follows:

$$NDTW(A,H) = \frac{DTW(A,H)}{|A| + |H|} \tag{18}$$

where $|\cdot|$ is the magnitude of a dataset.

The measurements of the driving behaviors have different units and need to be normalized to unitless quantities within the same range (e.g., [0, 1]) for comparison purposes. Therefore, a unity-based normalization method is adopted in this study. The maximum and minimum values of each measurement set will act as inputs. Because these inputs will be susceptible to abnormal values, the three-sigma rule of thumb is used to remove any outliers before conducting the unity-based normalization. Accordingly, this study uses the **unity-based normalized DTW distance (UNDTW)** defined below for the analysis in later sections:

$$UNDTW(A,H) = \frac{\widetilde{NDTW}(A,H) - \widetilde{NDTW}(A,H)_{min}}{\widetilde{NDTW}(A,H)_{max} - \widetilde{NDTW}(A,H)_{min}} \tag{19}$$

where $\widetilde{NDTW}(A,H)$ is the length-normalized DTW distance without outliers determined by the three-sigma rule of thumb.

In summary, in quantifying the behavioral differences, the DTW analysis framework can better capture the matching patterns and can relax the assumption of identical data length, compared with Euclidean distance. The DTW formulation is reduced to a shortest path problem, which is solvable in polynomial time using DP. More numerical results and analyses will be presented in the Results and Analysis section.

Model-Based Method: Stochastic Car-Following Models

The major questions this study aims to address are whether commonly applied models are able to capture the behavioral change in human drivers identified in Rahmati et al. (*18*), and if not, how to extend the original models to accommodate the changes. Car-following behavior has been studied extensively. Most commonly used car-following models are deterministic, with deliberately designed structures and parameter settings, and they include the intelligent driver model (IDM) (*28*), Gipps' model (*29*), and Newell's car-following model (*30*). Although these models have been developed with refined properties, they may not capture the intrinsic uncertainty of human drivers. To this end, several stochastic extensions of these models have been developed. For example, the parsimonious car-following model (*31*) added white acceleration noise to Newell's car-following model to address random errors in drivers' acceleration processes.

This study utilizes the IDM (*28*) and its stochastic version proposed by Treiber and Kesting (*32*) as representatives of deterministic and stochastic car-following models. Note that the analyses presented in the next section can be replicated with any car-following model. The model specifications are presented in the following equations:

$$a_n(t) = a_{max}\left[1 - \left(\frac{v_n(t)}{v_{des}}\right)^4\right] - a_{max}\left(\frac{s_{min} + v_n(t)T_{des} + \frac{v_n(t)\Delta v_n(t)}{2\sqrt{a_{max}b_{des}}}}{x_{n+1}(t) - l_{n+1}(t) - x_n(t)}\right)^2$$

where n represents the n^{th} vehicle, and $n+1$ is its leader, $a_n(t)$ is the acceleration of vehicle n at time t, $v_n(t)$ is the speed of vehicle n at time t, $\Delta v_n(t)$ is the relative speed, computed as $v_n(t) - v_{n+1}(t)$, $x_n(t)$ is the longitudinal location of vehicle n at time t, $l_{n+1}(t)$ is the length of the leading vehicle at time t, v_{des} is the desired speed, t_{des} is the desired time headway, s_{min} is the minimum physical gap between the leader and the follower, a_{max} is the maximum acceleration, and b_{des} is the desired deceleration m/s^2.

v_{des} (km/hr), t_{des} (sec), s_{min} (m), a_{max} (m/s^2), and b_{des} (m/s^2) are the parameters to be calibrated. To do so, the study follows the method designed in Hamdar (*33*) and chooses the mean absolute percentage error (MAPE) of speed as the metric, computed as follows:

$$MAPE_v = \frac{1}{N}\sum_{i=1}^{N}\left|\frac{v^i_{obs} - v^i_{sim}}{v^i_{obs}}\right| \times 100 \tag{21}$$

where v^i_{obs} is the observed speed from the car-following experiment, and v^i_{sim} is the speed calculated based on the calibrated IDM.

To minimize the MAPE of speed, this study uses a genetic algorithm because of the nonlinearity in the objective function. Moreover, as a metaheuristic method, genetic algorithms have good converge performance. To analyze further how stochasticity influences the model's ability to capture the behavioral change, this study adopts the stochastic IDM from Treiber and Kesting (*32*) and Bhattacharyya et al. (*34*), and uses the parameter σ_{IDM} to model the stochasticity of an individual driver explicitly. This paper assumes the distribution of the output acceleration is a normal distribution, given by

$$a \sim N\left(a|a_{IDM}, \sigma^2_{IDM}\right) \tag{22}$$

where a_{IDM} and σ_{IDM} are the mean and standard error, respectively. From the vehicle kinematics, we have:

$$v_{t+1} = v_t + a_t\Delta t \tag{23}$$

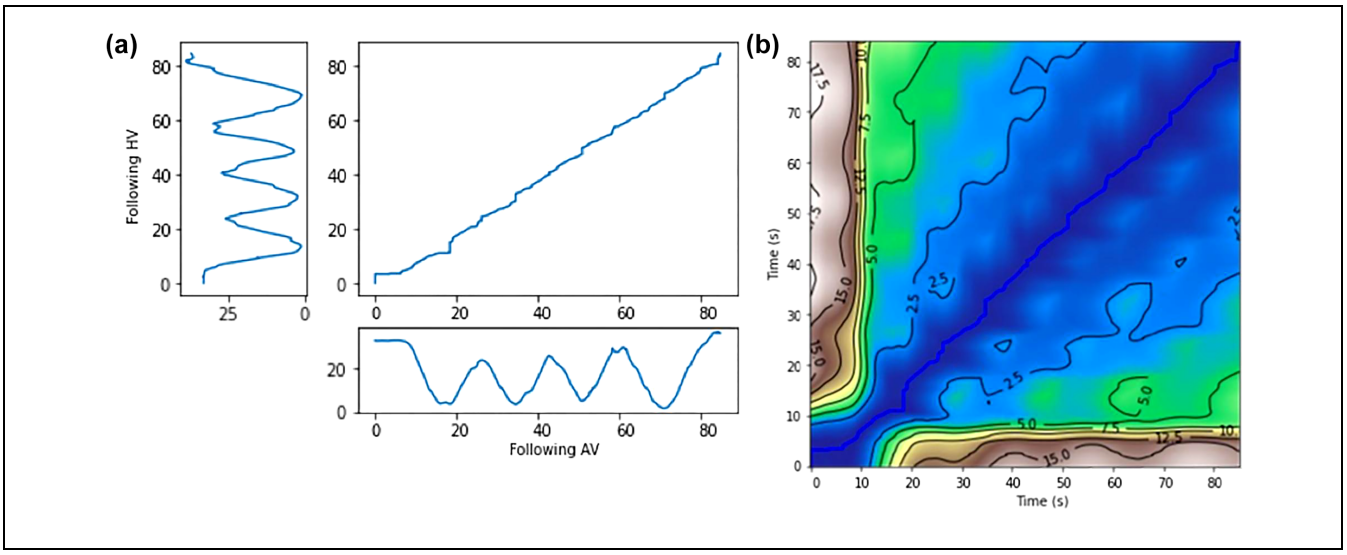

Figure 5. A demonstration on computing the warping path in DTW: (*a*) three-way plot, with the two speed time series placed perpendicularly and the warping path displayed in the center; and (*b*) density plot, with the local cost matrix displayed in the heat map and the corresponding warping path shown as a blue line.
Note: DTW = dynamic time warping; HV = human-driven vehicle; AV = automated vehicle.

where Δt is the unit time ($\Delta t = 0.1sec$ in this study). We can then derive the speed distribution from Equations 22 and 23, according to:

$$v_{t+1} \sim N\left(v_t + a_{IDM}\Delta t, \Delta t^2 \sigma_{IDM}^2\right) \tag{24}$$

where a_{IDM} is calculated based on Equation 20. σ_{IDM} is calibrated to minimize the MAPE of speed over 10 simulation runs with independent random seeds, following the similar routine described in Treiber and Kesting (*32*).

It is worth noting that the performance measure can be set at speed or spacing, and previous research suggests that calibrating deterministic models against spacing also yields acceptable results (*35*, *36*). However, the stochastic extension of IDM proposed by Treiber and Kesting (*32*) provides a distribution of speed explicitly, and if the simulated spacing were to compute numerically, a quadrature error would be introduced when evaluating the location at each time step. Therefore, to ensure consistency when calibrating the deterministic and stochastic IDM models, this study uses speed as the performance measure following the calibration process introduced by Treiber and Kesting (*32*). The calibration and validation results will be presented in the next section.

Results and Analysis

The primary goal of this study is to analyze the changes in human driver behavior in a mixed-autonomy traffic environment and to evaluate whether commonly used models are capable of capturing such changes. To this end, we designed a data-driven DTW analysis framework and take the IDM as an example to address the importance of stochasticity based on nonparametric hypothesis tests.

DTW

The power of DTW comes from finding the optimal matching patterns before calculating the sum of errors. Thus, the core is to find the warping path W. A sample from the collected speed data (driver 1 under speed profile 334 [*18*]) is provided to illustrate how the optimal matching pattern is computed. Figure 5*a* is a three-way plot, and the warping path in the center shows the mapping between the two cases: following an AV or another human-driven vehicle. The path in the plot is a continuous line starting from the origin and extending upward to the right until the end. This finding also provides validation of the proposed algorithm in obeying all three assumptions about DTW presented in the Methodology section. Figure 5*b* is a density plot, which uses a heat map to visualize the local cost matrix $D \in \mathbb{R}^{m \times n}$. Going from the bottom left to the upper right corner, the path with the least total cost is going to be the one drawn in blue, which chooses to go through the "valley."

Figure 6 shows an example of how a human driver reacts with respect to the leader's speed. The shift along the time axis in the follower's speed curve between the two cases can be observed, especially between 20 and 40 s from the start of the experiments. Such a phenomenon may be explained by the difference in driving behavior of

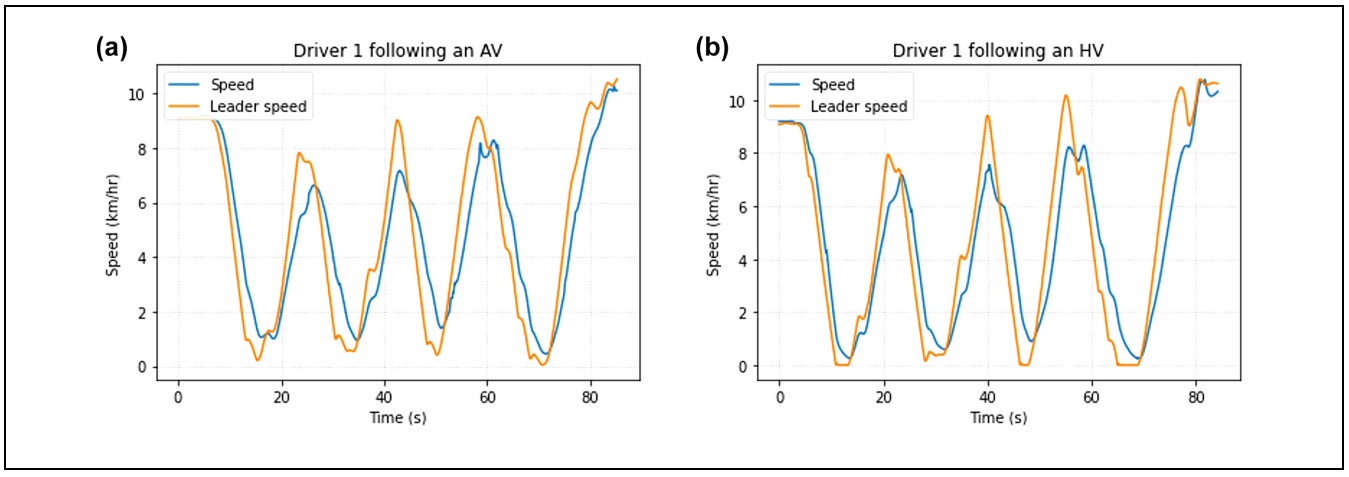

Figure 6. Speed and the leader's (driver 1) speed under speed profile 334: (*a*) following an AV; and (*b*) following a human-driven vehicle.
Note: AV = automated vehicle; HV = human-driven vehicle.

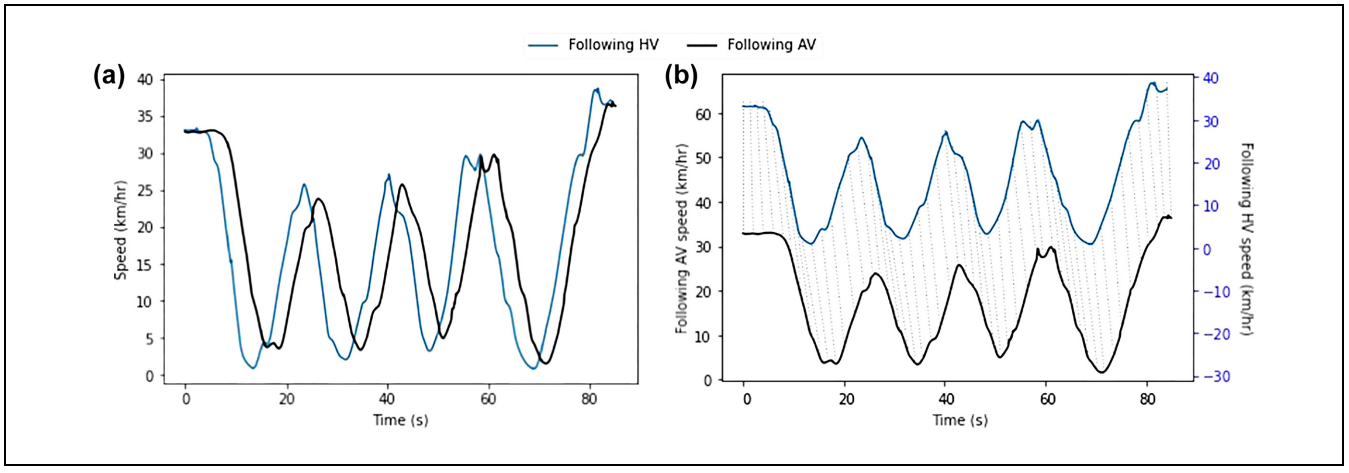

Figure 7. A demonstration of the matching patterns from the DTW analysis on speed: (*a*) original plot; and (*b*) plot with 30 unit offsets for the following AV case.
Note: DTW = dynamic time warping; AV = automated vehicle; HV = human-driven vehicle.

AVs and human-driven vehicles and the human response to this. The DTW analysis framework proposed in this study will first find the matching patterns and align the two time series data before evaluating the differences. This approach will address the time shift issue because of possible errors in time recording that occurred during data collection. Figure 7 further shows what the matching patterns look like. The two speed–time curves have very similar patterns and extreme values. Thus, to demonstrate the alignment better, an offset of 30 is added to the following AV case and the dotted lines present the matching between the two speed time series data.

Following the same analysis framework, the normalized DTW distance of five data categories is calculated and shown in Figure 8. A total of 44 drivers–speed profile pairs are investigated, and among all five behavior categories, the spacing evidently has a larger distance, which can be interpreted as a more significant difference in maintaining spacing when the leading vehicle is an AV or not. This is not detectable when looking at the aggregated descriptive statistics of spacing. Mahdinia et al. (*37*) conducted such an analysis on the same data set, and based on their results, we do not have sufficient evidence to say the spacing has a statistically significant difference when following an AV as opposed to a human-driven vehicle. This may be a result of neglecting the time series properties in the analysis of descriptive statistics. On the contrary, acceleration has the poorest performance in capturing the changes in human behavior. Acceleration often acts as the output in car-following models, and is rather insensitive to the desired speed and the parameters controlling the gaps (spacing and time

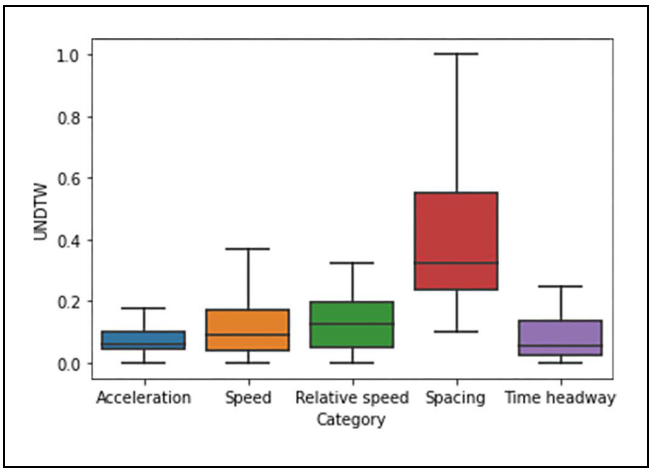

Figure 8. Boxplot showing the unity-based normalized DTW distance with different data categories.
Note: DTW = dynamic time warping; UNTDW = unity-based normalized dynamic time warping distance.

headway in the case of this study), according to Treiber and Kesting (*38*). The dispersion of speed and relative speed are similar to each other in Figure 8. This phenomenon can be predicted if speed and relative speed are strongly linearly correlated, which happens in stable traffic in which the leading vehicle has almost a constant speed.

The DTW analysis can also detect abnormal values in the data set. For example, one of the outliers of time headway is from the experiment of driver 2 under speed profile 211 (*18*). Figure 9*a* depicts a regular headway time series under speed profile 211. However, in Figure 9*b*, the vehicle has a headway of more than 500 s and should be removed in the following model-based method when calibrating the car-following models. The DTW analysis framework mentioned above was developed from a Python package called dtw (*27*). In summary, 85 driver–speed profiles were selected for the following study.

Stochastic IDM

Evidence from previous studies and the above analysis shows that human drivers' behavior will change when interacting with AVs in mixed traffic flow. The rest of this paper will calibrate and validate the IDM car-following model, which has been widely applied in previous research and used by existing simulation platforms. In this study, the IDM and stochastic IDM are calibrated with a genetic algorithm. The population is initialized with 30 parents and 900 child chromosomes. The mutation rate is 10% and Figure 10 shows the MAPE converges to less than 10% after 20 generations.

The distribution of the parameters calibrated for the IDM and the corresponding kernel density estimation are shown in Figure 11. The parameters can easily be perceived as not normally distributed based on the histograms, which violates the assumption of the *t*-test. Therefore, to determine if the distribution of the

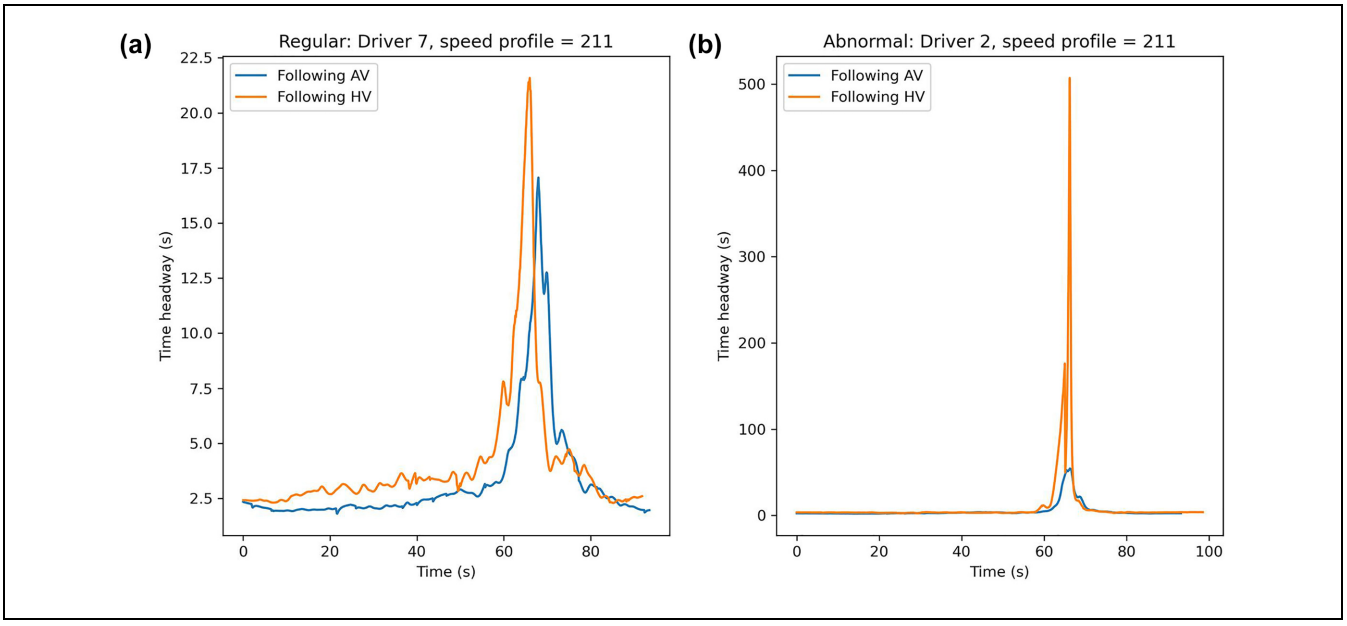

Figure 9. Comparison of headway data: (*a*) regular headway under speed profile 211; and (*b*) the outlier identified by DTW analysis.
Note: DTW = dynamic time warping; AV = automated vehicle; HV = human-driven vehicle.

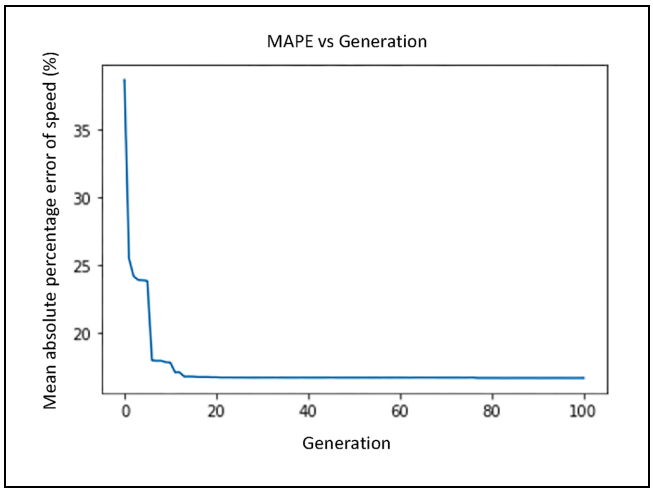

Figure 10. Convergence over generations in a genetic algorithm.
Note: MAPE = mean absolute percentage error.

parameters for human drivers' behavior when following an AV is significantly different from the distribution of the parameters when following a human-driven vehicle, the two-sample Kolmogorov–Smirnov (K–S) test is conducted on 85 realizations (42 from following a human-driven vehicle and 43 from following an AV). The hypothesis testing results are summarized in Table 2. The null hypothesis H_0 for both models is the same: the driving behavior parameters when following an AV and a human-driven vehicle are no different. Between the two models, all the parameters in the deterministic IDM (model 1) do not reject the null hypothesis, meaning we do not have sufficient confidence to say they are different. Combining the findings from the DTW analysis and the literature, the behavioral change is not captured by the IDM. As for the stochastic IDM (model 2), the *p*-value for σ_{IDM} is less than 0.01, and the null hypothesis is rejected, which means two σ_{IDM} are not from the same

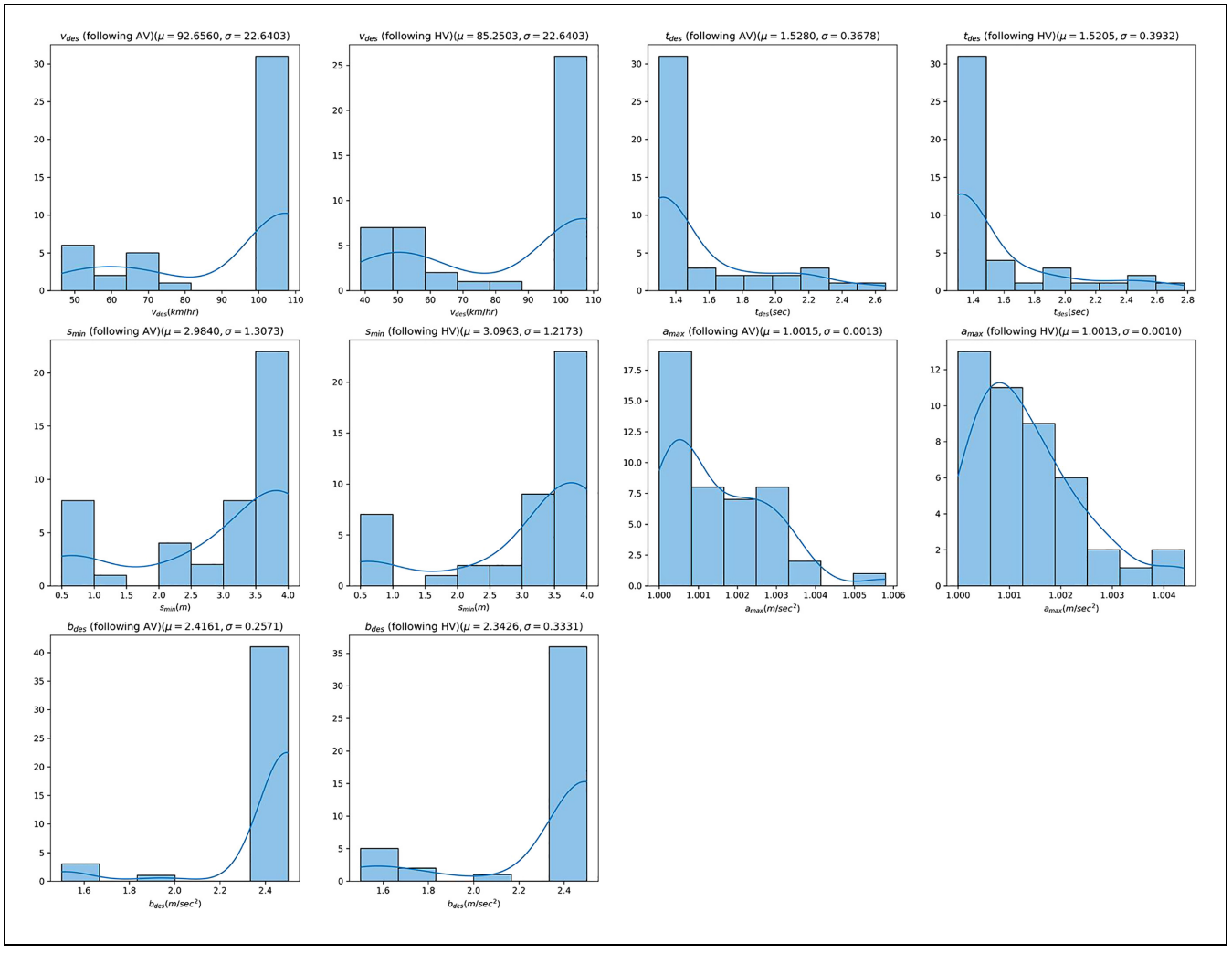

Figure 11. The distributions of IDM parameters.
Note: IDM = intelligent driver model; AV = automated vehicle; HV = human-driven vehicle.

Table 2. K–S Test Results

	Following HV			Following AV			K–S test
	Mean	SD	Obs.	Mean	SD	Obs.	*p*-value
Model 1: IDM							
v_{des}	85.2503	27.7736	42	92.6560	22.6403	43	0.3432
t_{des}	1.5205	0.3932	42	1.5280	0.3678	43	0.9821
s_{min}	3.0963	1.2173	42	2.9840	1.3073	43	0.7993
a_{max}	1.0013	0.0010	42	1.0015	0.0013	43	0.6094
b_{des}	2.3426	0.3331	42	2.4161	0.2571	43	0.2823
Model 2: stochastic IDM							
v_{des}	86.0557	26.3680	42	94.8700	19.9632	43	0.1694
t_{des}	1.5254	0.3766	42	1.5322	0.3369	43	0.1804
s_{min}	2.9361	1.2132	42	2.8247	1.2661	43	0.7992
a_{max}	1.0187	0.0163	42	1.0144	0.0131	43	0.4393
b_{des}	2.4054	0.2252	42	2.3948	0.2526	43	0.9952
σ_{IDM}	0.3812	0.0824	42	0.1090	0.0492	43	< 0.0001

Note: IDM = intelligent driver model; HV = human-driven vehicle; AV = automated vehicle; K–S = Kolmogorov–Smirnov; SD = standard deviation; obs. = observations. This shaded cell is to highlight the last parameter is the only one that rejects the null hypothesis.

distribution under a 99% confidence level. As shown in Table 2, drivers have a statistically significant lower level of uncertainty when following an AV, compared with following a conventional car. This result is further elaborated by the cumulative distribution functions (CDFs) in Figure 12. The hypothesis test results and corresponding *p*-values are listed above, and a clear gap is presented in the CDF plot of σ_{IDM}.

This finding provides validation of the methodology presented in the Methodology section, that is, employing a stochastic extension of deterministic models to address the changes in human behavior in mixed traffic. This also suggests that whenever the IDM is used to model AV–human-driven vehicle interactions, caution should be exercised because it may not capture the behavioral changes in human drivers.

Conclusion and Discussion

With the associated advances in sensing, computing, navigation, and control technology, AVs have drawn significant attention from both researchers and practitioners and have made an impact beyond the transportation arena. However, because of the low degree of public acceptance and other critical deployment issues, there is still a long way to go before a fully autonomous transportation system will be operational, especially for road traffic. Instead, it is expected that there will be a mixed traffic environment with different levels of autonomy. It has been perceived that human driving behavior will change in response to AVs, but whether existing models can capture such behavioral changes has not received proper investigation.

With a focus on car-following behavior, this paper uses a data set collected from human drivers' car-following behavior when following an AV (*18*). Two approaches were adopted: a data-driven method based on DTW; and a model-based method introducing stochasticity to the existing models.

For the data-driven method, this paper developed a robust DTW analysis framework, which first calculates the optimal matching between two behavioral time series data, and then uses the normalized DTW distance to quantify behavioral changes in human drivers. Next, we follow the same routine with other drivers' behavior recorded in the data set, including acceleration, speed, relative speed, time headway, and spacing (*18*). The results show that spacing has the best performance in measuring changes in human drivers' behavior, whereas there is little difference in acceleration between the two scenarios.

In the model-based analysis, a genetic algorithm is used to calibrate the IDM by minimizing the MAPE. The calibrated parameters of the IDM do not obey normal distributions, so to assess whether the parameters of the IDM are different when the leader is an AV, this paper uses a two-sample K–S test. The hypothesis testing shows parameters defined in the IDM cannot capture the behavioral changes. Thus, an extended IDM that explicitly models the stochasticity when a driver performs acceleration (*32*, *34*) is calibrated using a similar approach. Then K–S test result shows that the newly introduced parameter σ_{IDM} is different when following an AV as opposed to a conventional car. Drivers who follow an AV will have a lower level of uncertainty when driving.

This study introduces a new perspective on a DTW-based method for measuring the changes in drivers'

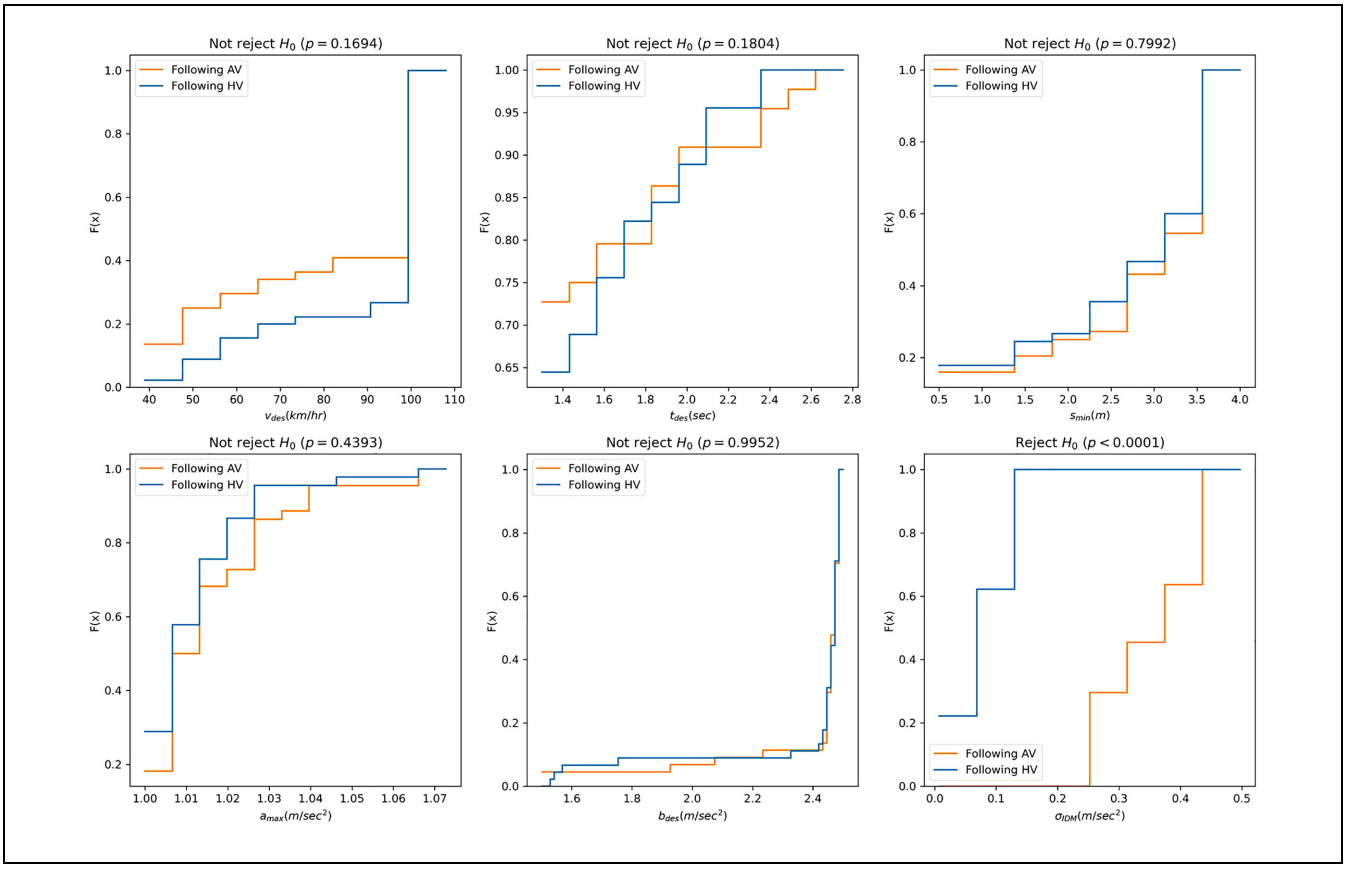

Figure 12. Cumulative distribution function for the six parameters in the stochastic IDM.
Note: IDM = intelligent driver model; AV = automated vehicle; HV = human-driven vehicle.

behavior when interacting with AVs. It is worth noting that the original DTW proposed by Bellman and Kalaba (*23*) does not account for the correlation in multivariate time series. However, the driving behavior measurements have correlations. For example, the spacings and relative speeds have high correlations, and applying DTW directly may risk losing correlation information. Bankó and Abonyi (*39*) and Hosseini et al. (*25*) discussed the potential for using feature selection methods to address this problem. For future research, orthogonalization methods, for example, principal component analysis, may be applied to construct new uncorrelated features before conducting the DTW analysis described in the Methodology section.

This study also heralds a new chapter of research in the area of investigating whether widely-adopted models can capture changes in human drivers' behavior in response to AVs. Thus, more models will be tested to identify the common features a model should possess to characterize the interactions in mixed-autonomy traffic. Finally, lane-changing behavior and other more complex interactions still remain undiscovered, and offer considerable potential for research.

Acknowledgments

The authors thank Dr.Yalda Rahmati at General Motors LLC for providing the data set used in this paper and for the discussion and collaborations that have guided us to this interesting problem.

Author Contributions

The authors confirm contribution to the paper as follows: study conception and design: Y. Zhang, A. Talebpour; data collection: A. Talebpour; analysis and interpretation of results: Y. Zhang, A. Talebpour; draft manuscript preparation: Y. Zhang, A. Talebpour. All authors reviewed the results and approved the final version of the manuscript.

Declaration of Conflicting Interests

The author(s) declared no potential conflicts of interest with respect to the research, authorship, and/or publication of this article.

Funding

The author(s) disclosed receipt of the following financial support for the research, authorship, and/or publication of this article: This material is based on work supported by the National Science Foundation under grant no. 2047937.

ORCID iDs

Yanlin Zhang https://orcid.org/0000-0002-5342-2755
Alireza Talebpour https://orcid.org/0000-0002-5412-5592

References

1. Fagnant, D. J., and K. Kockelman. Preparing a Nation for Autonomous Vehicles: Opportunities, Barriers and Policy Recommendations. *Transportation Research Part A: Policy and Practice*, Vol. 77, 2015, pp. 167–181.
2. Wang, L., H. Zhong, W. Ma, M. Abdel-Aty, and J. Park. How Many Crashes Can Connected Vehicle and Automated Vehicle Technologies Prevent: A Meta-Analysis. *Accident Analysis & Prevention*, Vol. 136, 2020, Article 105299.
3. Al Najada, H., and I. Mahgoub. Autonomous Vehicles Safe-Optimal Trajectory Selection Based on Big Data Analysis and Predefined User Preferences. *Proc., IEEE 7th Annual Ubiquitous Computing, Electronics & Mobile Communication Conference (UEMCON)*, New York City, 2016. IEEE, New York, 2016, pp. 1–6.
4. Talebpour, A., and H. S. Mahmassani. Influence of Connected and Autonomous Vehicles on Traffic Flow Stability and Throughput. *Transportation Research Part C: Emerging Technologies*, Vol. 71, 2016, pp. 143–163.
5. Patella, S., F. Scrucca, F. Asdrubali, and S. Carrese. Carbon Footprint of Autonomous Vehicles at the Urban Mobility System Level: A Traffic Simulation-Based Approach. *Transportation Research Part D: Transport and Environment*, Vol. 74, 2019, pp. 189–200.
6. Stern, R. E., Y. Chen, M. Churchill, F. Wu, M. L. Delle Monache, B. Piccoli, B. Seibold, J. Sprinkle, and D. B. Work. Quantifying Air Quality Benefits Resulting from Few Autonomous Vehicles Stabilizing Traffic. *Transportation Research Part D: Transport and Environment*, Vol. 67, 2019, pp. 351–365.
7. Talavera, E., A. Díaz-Álvarez, F. Jimènez, and J. E. Naranjo. Impact on Congestion and Fuel Consumption of a Cooperative Adaptive Cruise Control System with Lane-Level Position Estimation. *Energies*, Vol. 11, No. 1, 2018, p. 194. https://www.mdpi.com/1996-1073/11/1/194
8. Cohn, J., R. Ezike, J. Martin, K. Donkor, M. Ridgway, and M. Balding. Examining the Equity Impacts of Autonomous Vehicles: A Travel Demand Model Approach. *Transportation Research Record: Journal of the Transportation Research Board*, 2019. 2673: 23–35.
9. León, L. F. A., and Y. Aoyama. Industry Emergence and Market Capture: The Rise of Autonomous Vehicles. *Technological Forecasting and Social Change*, Vol. 180, 2022, Article 121661.
10. Litman, T. *Autonomous Vehicle Implementation Predictions: Implications for Transport Planning*. Victoria Transport Policy Institute, Victoria, BC, Canada, 2020.
11. Rajamani, R., and S. E. Shladover. An Experimental Comparative Study of Autonomous and Co-operative Vehicle-Follower Control Systems. *Transportation Research Part C: Emerging Technologies*, Vol. 9, No. 1, 2001, pp. 15–31.
12. Chen, D., S. Ahn, M. Chitturi, and D. A. Noyce. Towards Vehicle Automation: Roadway Capacity Formulation for Traffic Mixed with Regular and Automated Vehicles. *Transportation Research Part B: Methodological*, Vol. 100, 2017, pp. 196–221.
13. Van Arem, B., C. J. Van Driel, and R. Visser. The Impact of Cooperative Adaptive Cruise Control on Traffic-Flow Characteristics. *IEEE Transactions on Intelligent Transportation Systems*, Vol. 7, No. 4, 2006, pp. 429–436.
14. Wang, M., W. Daamen, S. P. Hoogendoorn, and B. van Arem. Rolling Horizon Control Framework for Driver Assistance Systems. Part II: Cooperative Sensing and Cooperative Control. *Transportation Research Part C: Emerging Technologies*, Vol. 40, 2014, pp. 290–311.
15. Cui, S., B. Seibold, R. Stern, and D. B. Work. Stabilizing Traffic Flow via a Single Autonomous Vehicle: Possibilities and Limitations. *Proc., IEEE Intelligent Vehicles Symposium (IV)*, Los Angeles, CA, 2017. IEEE, New York, 2017, pp. 1336–1341.
16. Stern, R. E., S. Cui, M. L. Delle Monache, R. Bhadani, M. Bunting, M. Churchill, N. Hamilton, et al. Dissipation of Stop-and-Go Waves via Control of Autonomous Vehicles: Field Experiments. *Transportation Research Part C: Emerging Technologies*, Vol. 89, 2018, pp. 205–221.
17. Zhao, X., Z. Wang, Z. Xu, Y. Wang, X. Li, and X. Qu. Field Experiments on Longitudinal Characteristics of Human Driver Behavior Following an Autonomous Vehicle. *Transportation Research Part C: Emerging Technologies*, Vol. 114, 2020, pp. 205–224.
18. Rahmati, Y., M. Khajeh Hosseini, A. Talebpour, B. Swain, and C. Nelson. Influence of Autonomous Vehicles on Car-Following Behavior of Human Drivers. *Transportation Research Record: Journal of the Transportation Research Board*, 2019. 2673: 367–379.
19. Zheng, F., C. Liu, X. Liu, S. E. Jabari, and L. Lu. Analyzing the Impact of Automated Vehicles on Uncertainty and Stability of the Mixed Traffic Flow. *Transportation Research Part C: Emerging Technologies*, Vol. 112, 2020, pp. 203–219.
20. U.S. Department of Transportation. *Next Generation Simulation: US101 Freeway Dataset*. Technical Report. Federal Highway Administration, Washington, DC, 2007.
21. Esling, P., and C. Agon. Time-Series Data Mining. *ACM Computing Surveys (CSUR)*, Vol. 45, No. 1, 2012, pp. 1–34.
22. Rakthanmanon, T., B. Campana, A. Mueen, G. Batista, B. Westover, Q. Zhu, J. Zakaria, and E. Keogh. Searching and Mining Trillions of Time Series Subsequences under Dynamic Time Warping. *Proc., 18th ACM SIGKDD International Conference on Knowledge Discovery and Data Mining*, Beijing, 2012. Association for Computing Machinery, New York, 2012, pp. 262–270.
23. Bellman, R., and R. Kalaba. On Adaptive Control Processes. *IRE Transactions on Automatic Control*, Vol. 4, No. 2, 1959, pp. 1–9.

24. Senin, P. *Dynamic Time Warping Algorithm Review*. Information and Computer Science Department, University of Hawaii, Manoa, Vol. 855, 2008, pp. 1–23.
25. Hosseini, M. K., A. Talebpour, S. Devunuri, and S. H. Hamdar. An Unsupervised Learning Framework for Detecting Adaptive Cruise Control Operated Vehicles in a Vehicle Trajectory Data. *Expert Systems with Applications*, Vol. 208, 2022, Article 118060.
26. Sakoe, H., and S. Chiba. Dynamic Programming Algorithm Optimization for Spoken Word Recognition. *IEEE Transactions on Acoustics, Speech, and Signal Processing*, Vol. 26, No. 1, 1978, pp. 43–49.
27. Giorgino, T. Computing and Visualizing Dynamic Time Warping Alignments in R: The dtw package. *Journal of Statistical Software*, Vol. 31, 2009, pp. 1–24.
28. Treiber, M., A. Hennecke, and D. Helbing. Congested Traffic States in Empirical Observations and Microscopic Simulations. *Physical Review E*, Vol. 62, No. 2, 2000, pp. 1805–1824.
29. Gipps, P. G. A Behavioural Car-Following Model for Computer Simulation. *Transportation Research Part B: Methodological*, Vol. 15, No. 2, 1981, pp. 105–111.
30. Newell, G. F. A Simplified Car-Following Theory: A Lower Order Model. *Transportation Research Part B: Methodological*, Vol. 36, No. 3, 2002, pp. 195–205.
31. Laval, J. A., C. S. Toth, and Y. Zhou. A Parsimonious Model for the Formation of Oscillations in Car-Following Models. *Transportation Research Part B: Methodological*, Vol. 70, 2014, pp. 228–238.
32. Treiber, M., and A. Kesting. The Intelligent Driver Model with Stochasticity – New Insights into Traffic Flow Oscillations. *Transportation Research Procedia*, Vol. 23, 2017, pp. 174–187.
33. Hamdar, S. H. Modeling Driver Behavior as a Stochastic Hazard-Based Risk-Taking Process. Doctor dissertation. Northwestern University, 2009, pp. 158–168.
34. Bhattacharyya, R. P., R. Senanayake, K. Brown, and M. J. Kochenderfer. Online Parameter Estimation for Human Driver Behavior Prediction. *Proc., American Control Conference (ACC)*, Denver, CO, 2020. IEEE, New York, 2020, pp. 301–306.
35. Punzo, V., and F. Simonelli. Analysis and Comparison of Microscopic Traffic Flow Models with Real Traffic Microscopic Data. *Transportation Research Record: Journal of the Transportation Research Board*, 2005. 1934: 53–63.
36. Punzo, V., B. Ciuffo, and M. Montanino. Can Results of Car-Following Model Calibration Based on Trajectory Data Be Trusted? *Transportation Research Record: Journal of the Transportation Research Board*, 2012. 2315: 11–24.
37. Mahdinia, I., A. Mohammadnazar, R. Arvin, and A. J. Khattak. Integration of Automated Vehicles in Mixed Traffic: Evaluating Changes in Performance of Following Human-Driven Vehicles. *Accident Analysis & Prevention*, Vol. 152, 2021, Article 106006.
38. Treiber, M., and A. Kesting. Microscopic Calibration and Validation of Car-Following Models – A Systematic Approach. *Procedia-Social and Behavioral Sciences*, Vol. 80, 2013, pp. 922–939.
39. Bankó, Z., and J. Abonyi. Correlation Based Dynamic Time Warping of Multivariate Time Series. *Expert Systems with Applications*, Vol. 39, No. 17, 2012, pp. 12814–12823.